Available online at www.sciencedirect.com
SCIENCE DIRECT®
Advances in Space Research 37 (2006) 1749–1758
ADVANCES IN SPACE RESEARCH (a COSPAR publication)
www.elsevier.com/locate/asr

A characterization of the moon radiation environment for radiation analysis

R.K. Tripathi [a,*], J.W. Wilson [a], F.F. Badavi [b], G. De Angelis [c]

[a] NASA Langley Research Center, Hampton, VA 23681, USA
[b] Christopher Newport University, Newport News, VA 23606, USA
[c] Old Dominion University, Norfolk, VA 23508, USA

Received 11 August 2005; received in revised form 2 March 2006; accepted 2 March 2006

Abstract

The radiation environment found on the surface of the Moon is shown and applied to different possible lunar mission scenarios. Models for the primary particle environment to be found on the Moon due to galactic cosmic rays (GCR) and solar particle events (SPE) have been used, with solar modulation and surface backscattering patterns taken into account. The surface itself has been modeled as regolith and bedrock. Particle transport has been performed with both deterministic and Monte Carlo approaches. A good agreement is found between the two methods.

Keywords: Moon radiation environment; Lunar mission scenarios; Galactic cosmic rays; Solar particle events; HZETRN deterministic space radiation transport code

1. Introduction

On January 14, 2004 President George Bush set up a new vision for NASA. He articulated agency's vision for space exploration in the 21st Century, encompassing broad range of human and robotic missions including missions to Moon, Mars and beyond. As a result, there is a focus on long duration space missions. NASA, as ever, is committed to the safety of the missions and the crew. There is an overwhelming emphasis on the reliability issues for the mission and the habitat. The cost effective design of the spacecraft demands a very stringent requirement on the optimization process. Exposure from the hazards of severe space radiation in deep space long duration missions is an operational constraint. Thus protection from the hazards of severe space radiation is of paramount importance for new vision. It is envisioned to have long duration human presence in Moon for deep space exploration. Therefore, there is a compelling need to know the radiation environment in space, on the surface of Moon and lunar regolith aimed at long duration human presence in Moon (see discussions in Wilson et al., 1997, 2003; De Angelis et al., 2002a,c, 2004).

The ionizing radiation environment is fundamentally of two sources, the galactic cosmic rays (GCR) entering the solar system from local interstellar space and the particles associated with acceleration across the transition boundary from a large scale coronal mass ejection (CME) into the local interplanetary media (Reames, 1999) and also possible acceleration in the solar surface during a large disturbance (Shea and Smart, 1993). These solar related particles are discrete events associated with solar activity and are referred to as solar particle events (SPE). From a human protection perspective, the low-energy components such as anomalous cosmic rays (ACR) resulting from the acceleration of interstellar plasma across the shock boundary at the edge of the solar system and associated high-speed solar storm particles are unimportant. Mostly

* Corresponding author.
E-mail address: r.k.tripathi@larc.nasa.gov (R.K. Tripathi).

0273-1177/$30
doi:10.1016/j.asr.2006.03.016

the most energetic SPE able to be detected by ground-based neutron monitors on the Earth are of importance to humans in space (Wilson et al., 1999a). Both the GCR and SPE sources are modified by the interplanetary fields during their propagation within the solar system. The expanding solar wind provides a strong convective current balancing the inward drift of GCR causing a general decrease of the GCR intensity in approaching the sun, which changes in degree in proportion to solar activity. SPE propagation allows some expansion along the sectored interplanetary magnetic field allowing a decrease in intensity at larger distances. There is some evidence that the CME shock driven events weaken slowly over a few AU from the sun (Reames, 1999).

These sources are greatly modified near planetary bodies or large satellites (Wilson et al., 2000, 2003). Interaction with such large bodies effectively shields against the local space environmental components. In addition to the effect of shielding, secondary radiations are induced by collision of GCR and SPE with the body surface materials and/or atmosphere, adding to the local radiation field. Neutrons are a most conspicuous component since their short lifetime (11 min) limits their propagation from their collisional source and they are not a normal part of the deep space environment except for the induced field near a large body. If the body has a magnetic field, the dipole component makes an effective magnetic bottle in which the neutron charged decay products (electron and proton) could be trapped forming a belt of ionizing radiation centered on the magnetic equator such as seen for the Earth and Jupiter. In addition to the relatively stable trapped protons and electrons, the magnetic field interacts with the interplanetary plasma forming a bow shock and magnetic tail through which the interplanetary media is accelerated through inward radial diffusion leading to precipitation near the magnetic poles. In addition, the magnetic fields deflect energetic charged particles entering into magnetic equatorial regions so those particles of the interplanetary environment reach the planetary surface mainly near the magnetic poles.

This work reviews previous Langley activity on the lunar radiation environment (De Angelis et al., 2002a,b,c, 2004; Clowdsley et al., 2003; Wilson et al., 2003) and goes on to provide new characterization of the moon environment for radiation analysis using the deterministic approach. The moon profile (De Angelis et al., 2002a,b,c, 2004) is based on a detailed description of the lunar regolith and rocks from both the physical and chemical point of view as from a single lunar location, namely the Oceanus Procellarum landing site of the Apollo 12 mission, with the same chemical composition adopted for the whole Moon for both surface and rock layers, chosen as an average of the Apollo 12 surface samples taken at the Oceanus Procellarum landing site.

2. Environmental models

In this section the environmental models used are shown. First discussed is the SPE model and assumptions used, next is the GCR model (Badhwar and O'Neill, 1996). These Langley base models are used in our environmental models (e.g. Wilson et al., 1997, 2003; De Angelis et al., 2002a,b,c, 2004; Clowdsley et al., 2003).

2.1. Solar particle events

Solar particle events are composed mostly of protons and the rest of this paper concerns only the proton component.

2.1.1. Solar proton propagation

Solar proton events have been recorded at the earth since 1942 although the detection technique varied considerably over the last 50 years. Although solar flare process is assumed to be the source of SPE, recent studies indicate (Reames, 1999) that coronal mass ejection (CME) may be the source of SPE. It is almost a customary to refer to SPE as meaning from the solar flare, and as major solar flares are associated with CME, in this paper we would use 'solar winds' and CME interchangeably in the discussions of SPE. Solar winds are super ionized plasma coming from the corona of the sun. Solar propagation of SPE is closely intertwined (Meyer et al., 1956) with the magnetic topology of the interplanetary medium. The plasma flows radically from the sun. The interplanetary magnetic fields from the sun to earth 'appear' to be curved in the Archimedean spiral nature. The energy density of this plasma is much larger than the energy density of the interplanetary magnetic field, so for all practical purposes, it is assumed that the interplanetary magnetic field within the plasma is 'frozen'. The solar protons appear to propagate into the interplanetary medium through two independent phases. The first is the diffusion from the CME site through the corona to the 'foot' of the idealized Archimedean spiral path formed by the interplanetary magnetic field line between the sun and the detection point. The second phase is the propagation in the interplanetary medium from the sun to the detection point along the interplanetary magnetic field lines. The intensity is higher, rises faster and is for shorter duration if the point of observation is located along the interplanetary field line from the point of ejection in the sun at other locations the intensity is lower rises and decreases slowly and is therefore for longer durations.

2.1.2. Solar proton event characteristics

Solar proton events as measured at the orbit of the earth have common characteristics of a propagation delay between the onset of the solar flare/CME in electromagnetic emission and the onset of the particle increase, a rapid increase to the maximum intensity and a slow decay to the background (Shea and Smart, 1993). For a solar flare on the western portion of the sun, the solar particle flux usually rises and decays fairly rapidly compared to solar flare on the eastern hemisphere of the sun. In addition to the solar protons from the flare/CME that are visually observed from the earth, approximately 20 percent of

SPE detected at the earth have been associated with the activity invisible from the earth. These events pose a special problem for an interplanetary mission since earth-based observations can only see half of the sun. Had an interplanetary mission been located on the far side of the sun (as viewed from earth) and been connected to the flaring region via the interplanetary magnetic field lines, the spacecraft would have been subjected to a major SPE which would not have been anticipated by any earth-based measurements. For this reason, on-board optical, X-ray, and particle monitors would be essential equipment for manned interplanetary mission like Mars. In addition, techniques would have to be developed to predict an intensity-time profile for an interplanetary mission.

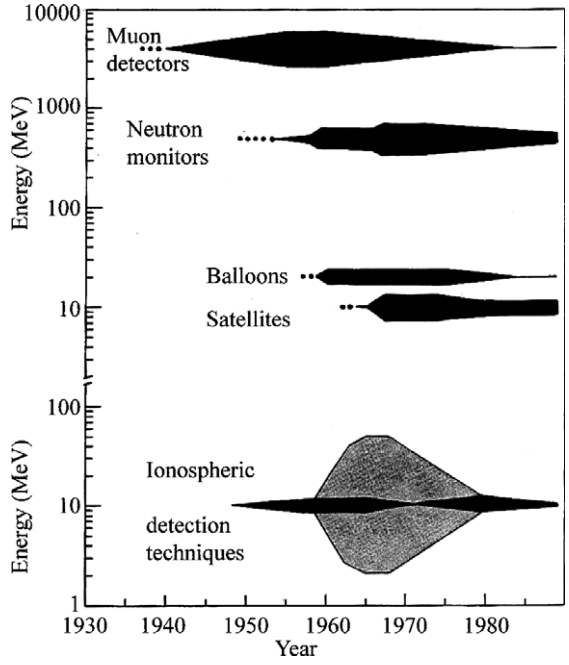

Fig. 1. History of SPE measurements (Shea and Smart, 1993).

At present time it is not possible to predict when a SPE is likely to occur. Initial SPE relied on ground-based measurements of secondary particles generated at the top of the earth's atmosphere. Sensors have been flown on balloons since International Geophysical Year (1957–1958), and on spacecrafts since the early 1960s. Fig. 1 gives a conceptual history (Shea and Smart, 1993) of the availability and energy threshold of each technique used to detect solar proton events since 1933. Presently spacecraft provide most reliable measurements.

As discussed in Fig. 1, earlier observations were mostly done at ground level on earth, and as a result, a considerable attention was given to the two SPE events, one of February 23, 1956 and the other of September 29, 1989 that produced significant signals on ion chambers or neutron monitors. In the February 23, 1956 occurrence neutron monitor count rates rose to 3600 percent above background levels (Fig. 2) and is the largest observed

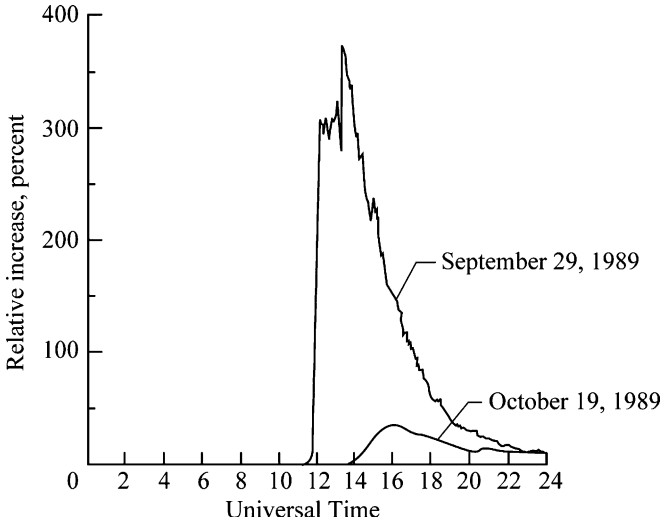

Fig. 3. Deep River neutron monitor count rates during the solar particle events of October 19 and September 29, 1989 (Tripathi et al., 2001).

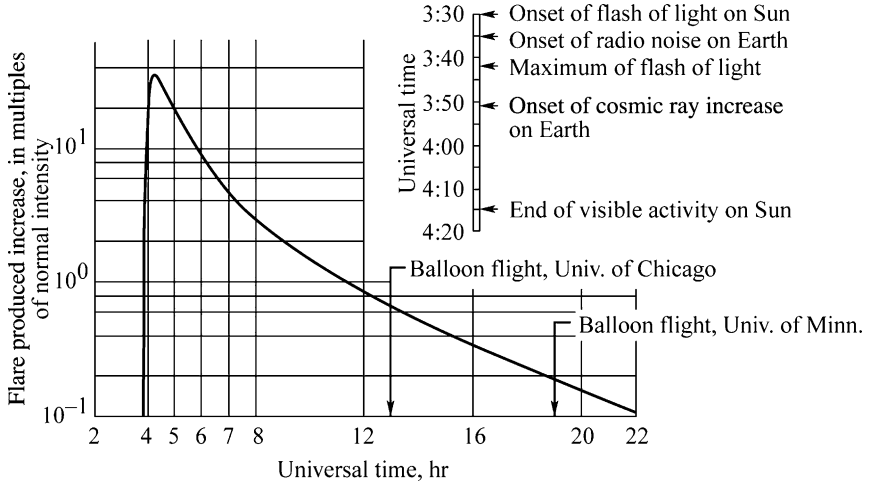

Fig. 2. Ground level neutron monitor event seen at Durham, NH on February 23, 1956 (Schaefer, 1959).

event on the ground during the last 60 years. The event of September 29, 1989 produced signals about 370 times over the background (Fig. 3) and is the next largest ground observed SPE. Higher energy ions produce events that are observable on the ground hence ground observations spectra are reliable at higher energies and are supplemented by satellite observations (mostly after 1960s) at lower energies. For this reason September 29, 1989 observations are more reliable at lower energies than February 23, 1956 event. The energy spectra of September 29, 1989 event was investigated by Nymmik (1996). The proton fluence for energies above 30 MeV was found to be given by

$$\int_{30}^{\infty} \phi(E)dE = 1.39 \times 10^9 \text{ protons/cm}^2, \quad (1)$$

where E is the kinetic energy and $\phi(E)$ is the differential fluence in protons/(cm^2-MeV) and is given as a power law in particle momentum (proportional to magnetic rigidity) above 30 MeV by

$$\phi(E)\mathrm{d}E = \frac{C}{\beta} \times \left(\frac{p(E)}{p_{30}}\right)^{-4.5} \mathrm{d}E, \quad (2)$$

where, $\beta(=p/\sqrt{\{(p^2 + (2mc^2)^2\}})$ is the proton velocity relative to the velocity of light, $p(E)$ is the momentum, $p_{30} = 239.15$ MV is the momentum corresponding to a proton energy of 30 MeV. The coefficient C is given by

$$C = \frac{1.39 \times 10^9}{\int_{30}^{\infty} \left(\frac{239.15}{p(E)}\right)^{4.5} \frac{1}{\beta}\mathrm{d}E} = 2.034 \times 10^7. \quad (3)$$

A good description of the differential fluence in protons/(cm^2-MeV) below 30 MeV has been given by using an exponential distribution (Shea and Smart, 1993), since there is a flattening of the spectra below that energy based upon observations of this event (Cleghorn and Badhwar, 1997). Both of these models together provide the event-integrated fluence for protons of the entire measured energy range for this event.

There is not much information about the radial dependence of SPE. Events may decrease very little between 1 AU to Mars orbit. The intensity is mainly determined by the diffusion process. At large distances from the sun, Gauss law is assumed appropriate. To make a gradual transition to the Gauss's law, perhaps, it is good to assume an inverse r dependence to 2 AU and Gauss law dependence beyond 2 AU, which is probably conservative. For design purposes, an event like 4× September 29, 1989 event (an event four times larger than the September 29, 1989 event, Wilson et al., 1999a), which is likely to be exceeded only 1 percent of the time (Xapsos et al., 1999), is used with the accounted radial dependence. The major SPEs during solar cycles 19–22 are given in Fig. 4. In addition to the SPEs discussed above, August 1972 dominates in the range of 70–100 MeV, which is important for radiation hazards of blood forming organs (BFO). It is worth mentioning that if a major SPE coincides with major geomagnetic storms (with a resulting sudden decrease in cutoff rigidity) earth orbiting spacecraft will experience an increased particle flux exposure for a few hours.

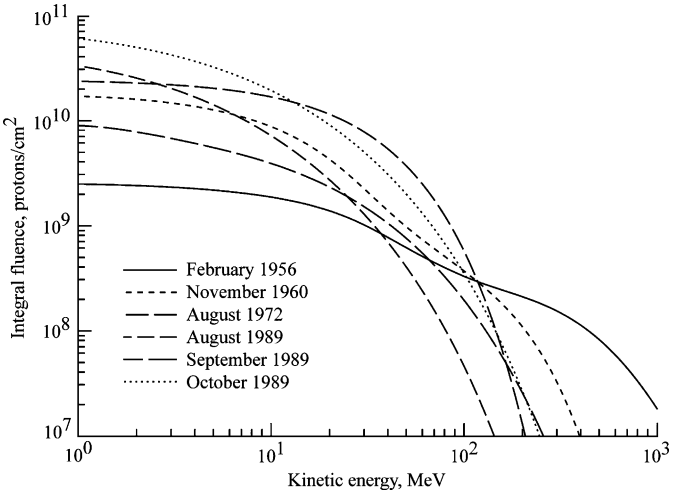

Fig. 4. Large SPEs integral flux at 1 AU during solar cycles 19–22 (Wilson et al., 1997).

2.2. Galactic cosmic rays

The exact process of the origin of cosmic rays in galaxy is not entirely known (Hall et al., 1996). In the solar system these interact with the outward propagating solar wind in which is embedded the solar magnetic field. By balancing the inward diffusion of the galactic cosmic rays and the outward convection by the solar winds Parker (1965) solved the Fokker–Planck equation. The density of cosmic ions within the solar system, assuming spherical symmetry, is then related to the external density as

$$\mu(r, R) = \mu_0(R)exp[-\int_r V(r')\mathrm{d}r'/D(r', R)], \quad (4)$$

where $D(r, R)$ is the diffusion coefficient (Balasubramanyan et al., 1967), $\mu(r, R)$ is the ion density at radial distance r and magnetic rigidity R (particle momentum per unit charge and determines the trajectory radius of curvature in a magnetic field), $\mu_0(R)$ is the density in interstellar space, and $V(r)$ is the solar wind speed. The wind velocity and diffusion coefficient depend on the solar activity. It is customary to measure the sun activity by the number of sunspots (Wolf sunspot number) observed in the solar surface (see discussion in Wilson et al., 1999b) and there is a phase shift between sunspot number and modulation as the wind generated at the solar surface diffuses into the modulation cavity which extends far out into the solar system.

On the surface of the earth cosmic ray neutron monitors are used to observe the relative cosmic ray intensity. The relation of sunspot number to the cosmic ray intensity as indicated by the relative counting rate high latitude neutron monitors is well established (Belov, 2000). For many

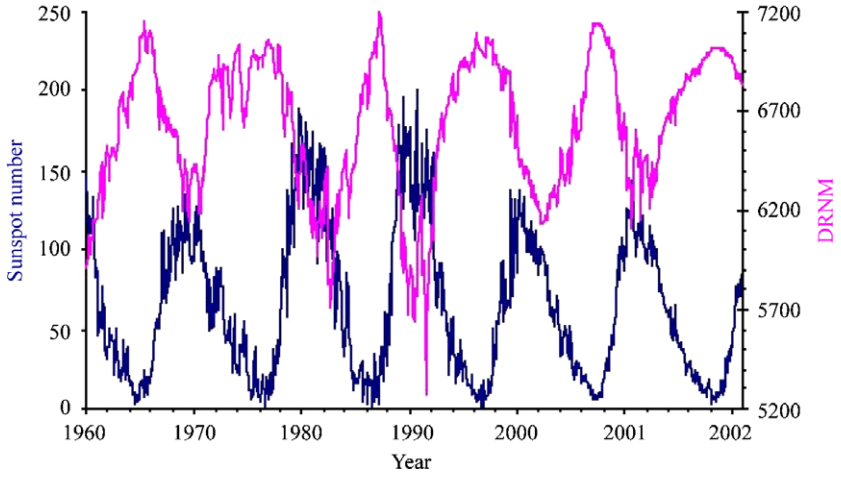

Fig. 5. The relation between the solar sunspot number and the Deep River neutron monitor count rate and its projection forward until 2022. (Wilson et al., 2003).

years until its closure in 1995, the high counting rate of the Deep River neutron monitor (with a 1 GV geomagnetic cutoff) was used to characterize the solar cycle modulation of the cosmic radiation. In Fig. 5 we have used all of the Deep River neutron monitor data to model the cosmic ray modulation. The inverse relation of solar activity and cosmic ray intensity is clearly seen in the figure. We have projected this model forward to indicate the expected relative cosmic ray modulation levels until the year 2022. Statistical models have been used to study the sunspot numbers (Wilson et al., 1999b, 2002). We note that the cycle is reasonably well determined soon after solar minimum but chaos enters late in the cycle and great uncertainty enters in cycle projections across the solar minimum. It is complex to include uncertainty from this chaos and is not included in the current projections. By making some assumptions Badhwar et al. (1994) simplified the Parker diffusion model version where they held solar wind at a constant value of 400 km/s and the diffusion coefficient was taken as a function of time and was correlated with the Mt. Washington neutron monitor count rate. In their investigation, the diffusion was found to be bimodal with unique dependence on the orientation of the solar magnetic dipole. Assuming an isotropic diffusion coefficient in which the diffusion coefficient generally increases with radial distance as $D(r,R) = D_0(R)\, r^s$ where s is on the order of 0–2, these assumptions lead to

$$\mu(r, R) = \mu_0(R) \exp\{-V_0(r_0^{1-s} - r^{1-s})/[(1-s)D_0(R)]\}, \quad (5)$$

where V_0, r_0, and $D_0(R)$ are the wind speed, size of the modulation cavity (50–100 AU), and diffusion coefficient at 1 AU, respectively. Eq. (5) is used to scale the modulated flux at 1 AU to arbitrary distance (Wilson et al., 1999b). Spacecrafts Pioneer, Voyager, and IMP have been used for modulation studies and indicate variability of s with solar cycle for some restricted energy ranges but the gross behavior for all energies above 70 MeV/amu is well represented by $s = 0.5$ (Fuji and McDonald, 1997).

Figs. 6 and 7 show the comparison of the simplified diffusion model of Badhwar et al. (1994) with measurements of selected GCR nuclei both for solar maximum and solar minimum. The low-energy part (below ~1 GeV) of the GCR is modulated by about a factor of two as the solar wind and magnetic field increases and decreases over the solar cycle. The most prominent particles are in a broad energy range between 100 and 1000 MeV/amu. These are very penetrating radiations able to penetrate deep into the Earth's atmosphere although only the most energetic particles produce effects at ground levels. A peculiarity of the GCR is the significant number of multiple charged ions (for example oxygen and iron ions in the figures). These multiple charged ions make large contributions to biological injury and single event effects in electronic devices. There has been a continuing effort over many years to measure and model GCR fluxes. Current models are believed to have accuracies of about 25 percent.

3. Moon profile

The details of the environmental model are described elsewhere (De Angelis et al., 2002a,b,c, 2003, 2004) and are not elaborated. Different sections for chemical and physical properties are given below.

3.1. Chemical composition of lunar regolith and bedrock

The environment at the surface and lunar regolith and bedrock depends on its chemical composition as the impacting radiation interacts differently with different chemical element. The Moon surface has been modeled as a 5 m regolith layer, followed by rock, with the same composition adopted for both surface and rock layers, chosen as an average of the Apollo 12 surface samples taken at the Oceanus Procellarum landing site (see De Angelis et al., 2002a,b,c for the analysis). The Table 1 shows this composition in percent mass.

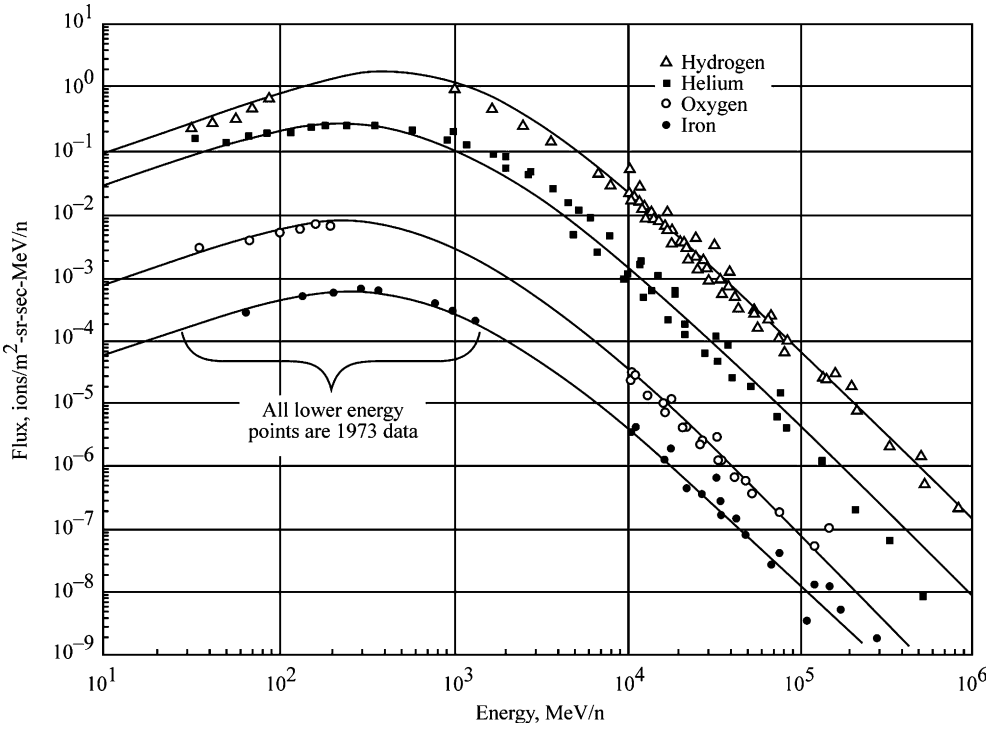

Fig. 6. Fit of the Fokker–Planck diffusion equation to 1973 differential energy spectra (Badhwar et al., 1994).

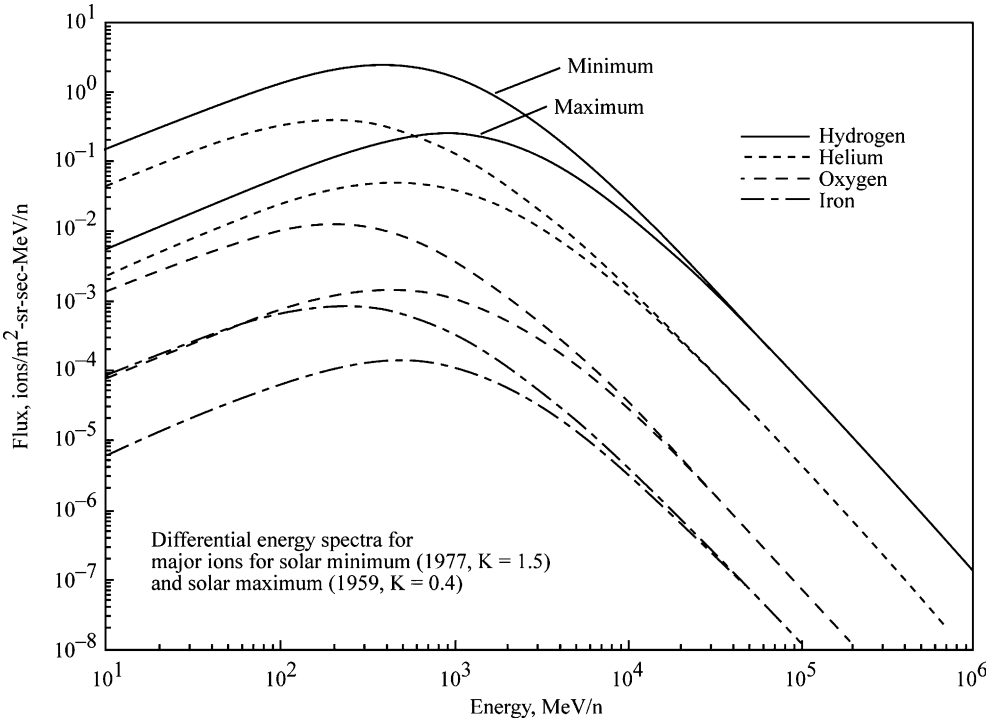

Fig. 7. 'Worst-case' differential energy spectra during solar minimum and solar maximum (Badhwar et al., 1994).

3.2. Lunar day and night temperature profile

The temperature profile in regolith and bedrock are different. Two different scenarios have been considered, namely a Lunar Night ($T_{surface} = 100$ K) and a Lunar Day ($T_{surface} = 400$ K) scenario, with temperature profiles for regolith and rock extrapolated from data from the Apollo 15 and Apollo 17 landing sites measurements (see De Angelis et al., 2002a,b for the analysis).

Table 1
Chemical composition of lunar regolith and bedrock (De Angelis et al., 2002c)

Chemical composition	In % mass
SiO_2	42.1
FeO	17.4
Al_2O_3	13.0
CaO	11.3
MgO	8.0
TiO_2	7.2
Cr_2O_3	0.27
MnO	0.20
Na	3150 (ppm)
K	1090 (ppm)

3.3. Lunar density profile

The Moon surface has been modeled as a 5 m regolith layer, followed by rock. The regolith density profile has been obtained by combining data from ground-based radiophysical measurements and from in situ analysis data from the Lunar, Surveyor and Apollo missions (the analysis is shown in De Angelis et al., 2002a,b), whereas for the rock layer a constant value of 3.3 g/cm^3 has been used as typical of mare basalt rock (De Angelis et al., 2002a,b).

3.4. Induced environments

The above formalism is for GCR and SPE in free space. The radiation environment gets considerably modified as one approaches a large object such as a planet or a satellite, the ambient radiation field is disturbed by interaction with the near body (Wilson et al., 2003). The modified environment is mainly due to the interaction of radiation with the materials of the neighboring objects' e.g. regolith, atmosphere etc. The incoming radiation gets absorbed, fragments, and produces new radiation particles that are not present in the free environment. The incoming ions also break up impacting target materials fragmenting them and producing additional radiation ions. There are several kinds of nuclear reactions take place that are responsible for producing the induced environment. Neutron is one of the secondary particles that is produced in these reactions, the produced neutrons diffuse into space providing a neutron albedo (to a lesser extent other particles as well) (Clowdsley et al., 2003; Wilson et al., 2003). If there is atmosphere in the approaching body then neutrons at the surface have been produced from two sources – with the interaction from the atmospheric particles and those diffusing from below by the planet regolith. If in addition the body has a dipole magnetic field then the composition of the radiation in trapped region would be modified as well. As it can capture the secondary decay particles as neutron decay products allowing the buildup of intense electron and proton belts about the body as in the case of Earth (Wilson et al., 2002) and Jupiter. The Earth neighborhood environment has been discussed elsewhere (Wilson et al., 2002).

3.5. Lunar neighborhood environment (lunar surface environment)

As discussed in the previous sections, the GCR and SPE are modified in the presence of other objects. Lunar surface environment is affected by the near Earth environment. These radiations impact the lunar surface producing various kinds of nuclear reaction thus fragmenting and producing secondary particles, which diffuse from the surface into the local environment. Besides, on interaction with the regolith additional radiation ions are produced as well. In addition the lunar mass shields the surface from directions intersecting the

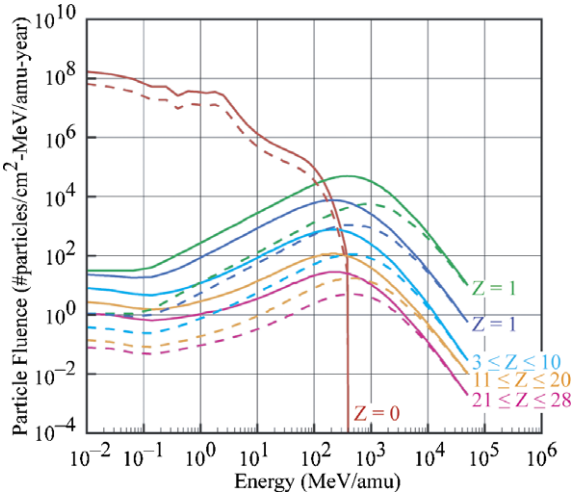

Fig. 8. GCR environment during the 1977 solar minimum (full lines) and the 1990 solar maximum (dashed lines) on the lunar surface (Clowdsley et al., 2003).

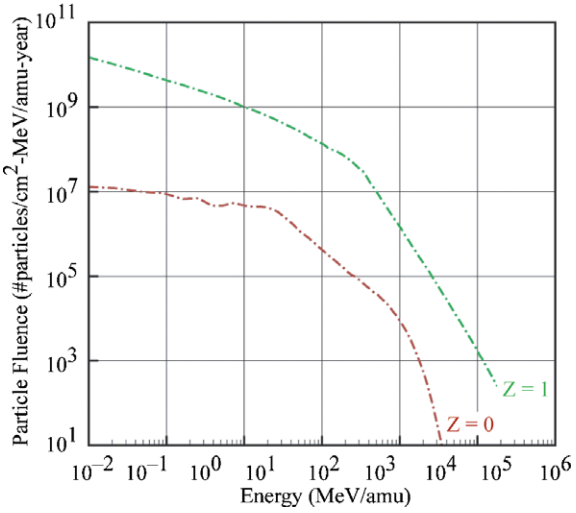

Fig. 9. The lunar surface environment during the September 1989 SPE (Clowdsley et al., 2003).

lunar terrain. In general, one may consider that the shielding effect is nearly a factor of two corresponding to all directions below the horizon. Regolith also can be used to protect human operations (Simonsen et al., 1990). In lunar orbit, the interactions with the lunar surface are absent, as a result the ions and secondary particles, in general produced by regolith decrease, and hence neutron albedo decreases as well. The Langley GCR environment on the lunar surface is shown in Fig. 8 at solar 1977 solar minimum and 1990 solar maximum (Clowdsley et al., 2003). Similar results are shown in Fig. 9 for the solar particle event of September 29,

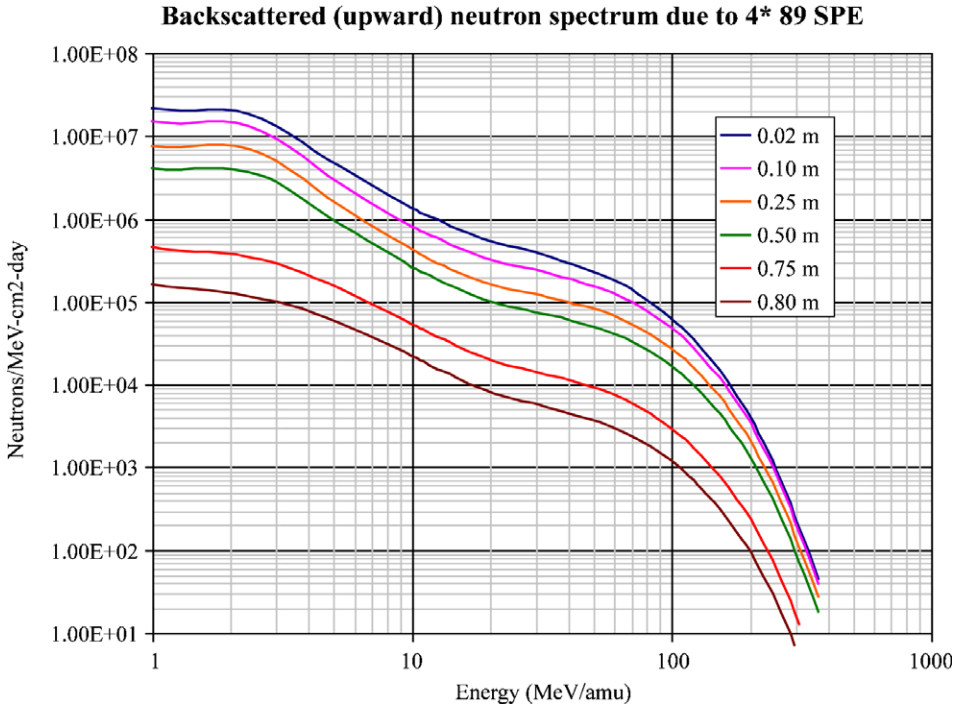

Fig. 10. Environment in regolith for 4* 1989 SPE.

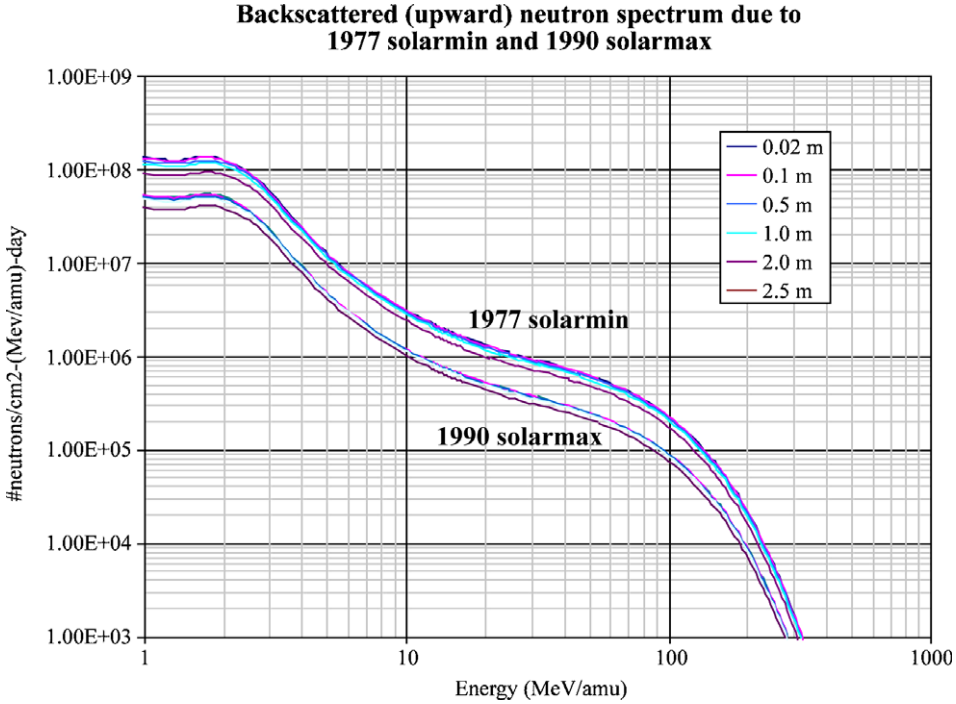

Fig. 11. Radiation environment in lunar regolith for 1977 solar minimum and 1990 solar maximum using HZETRN code.

1989 (Clowdsley et al., 2003). Note, the neutron albedo is completely dominated by the direct solar particles arriving from above the horizon. The difference between the results in Fig. 8 and in Fig. 9 is that for GCR there are more nuclear reactions producing the neutrons than in SPE (Clowdsley et al., 2003).

4. Environment in lunar regolith

The NASA Langley Research Center has developed a reliable deterministic particle transport code HZETRN for cosmic radiation ions through material targets (Wilson et al., 1995). This code solves Boltzmann equation and gives fluence, dose, dose equivalent and Gray equivalent at any depth of the material (Wilson et al., 2003). Results of transport for the same GCR and SPE primary particles performed with the HZETRN code with the lunar surface model are used in Langley studies. Fig. 10 shows the results of the deterministic approach for backscattered (upward) neutron spectrum for 4× September 1989 SPE as this is more reliable for design process than 1956 SPE spectrum due to the better accuracy of experimental measurements in 1989 (Tripathi et al., 2001). The Monte Carlo FLUKA studies (De Angelis et al., 2002a,b) also show that there are no backscattered neutrons for depth greater than 80 cm in regolith. This shows a good agreement between the deterministic and Monte Carlo transport approaches. The lack of backscattered neutron also means that regolith can work as a reasonably good shielding material for protection from SPE hazards.

Backscattered (upward) neutron spectra due to GCR 1997 solar minimum and 1990 solar maximum in lunar regolith in Langley deterministic approach is shown in Fig. 11. We note that there is not spread in the back scattered neutron spectra with regolith depth and that only backscattered neutrons due to GCR are present in regolith environment for depth greater than 80 cm, mainly due to the higher energy radiation ions in GCR incoming spectra. Similar results are found in the Monte Carlo FLUKA studies as well. Again this demonstrates a good agreement between the Langley deterministic and Monte Carlo FLUKA transport approaches for GCR studies as well. This also means that greater thickness of lunar regolith material is needed for the protection from the hazards of cosmic radiation.

Fig. 12 shows the GCR upward going neutrons using Monte Carlo code FLUKA (De Angelis et al., 2002a,b), as discussed earlier, these results are in good agreement with that of Fig. 11 obtained using Langley deterministic code HZETRN. Here also there is not much spread in the spectra with regolith depth. Non-spread of the spectra with regolith depth has origin, as pointed out before, due to the high-energy spectra of GCR.

5. Conclusions

A review of the radiation environment on the surface of Moon, in regolith for SPE and GCR spectra has been performed. The results show differences in the SPE and GCR spectra on the surface and in regolith. There is good agreement between the results shown for the deterministic and

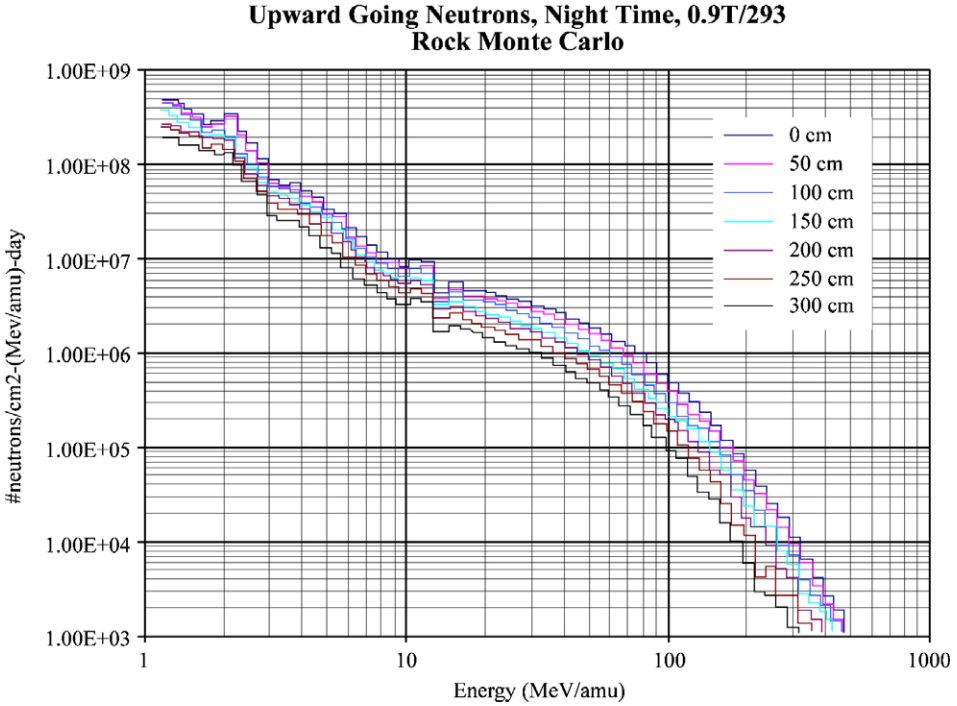

Fig. 12. Radiation environment in lunar regolith using Monte Carlo code FLUKA (results from De Angelis et al., 2002a).

Monte Carlo transport codes in regolith, increasing confidence in the radiation environment results. In view of the huge differences in the time and effort involved in the deterministic and Monte Carlo approaches, it is useful to carry out detailed studies in the deterministic approach.

References

Badhwar, G.D., Cucinotta, F.A., O'Neill, P.M. An analysis of interplanetary space radiation exposure for various solar cycles. Radiat. Res. 138, 201–208, 1994.

Badhwar, G.D., O'Neill, P.M. Galactic cosmic radiation model and its applications. Adv. Space Res. 17, 7–17, 1996.

Balasubramanyan, V.K., Bolt, E., Palmeira, R.A. Solar modulation of galactic cosmic rays. J. Geophys. Res. 72, 27–36, 1967.

Belov, A.V. Large scale modulation: view from the Earth. Space Sci. Rev. 93, 79–105, 2000.

Cleghorn, T.F., Badhwar, G.D. Comparison of the SPE model with proton and heavy ion data. Impact of Solar Energetic Particle Events for Design of Human Missions Workshop, September 9–11, 1997.

Clowdsley, M.S., De Angelis, G., Badavi, F.F., et al. Surface environments for exploration, in: El-Genk, M. (Ed.), Proceedings of the Space Technology and Application International Forum (STAIF-2003) 'Expanding the Frontiers of Science', AIP Conference Proceedings, New York, pp. 1034–1045, 2003.

De Angelis, G., Wilson, J.W., Clowdsley, M.S., et al. Lunar lava tubes radiation safety analysis. J. Radiat. Res. 43, S41–S45, 2002a.

De Angelis, G., Wilson, J.W., Clowdsley, M.S., et al. A radiation safety analysis for lunar lava tubes, in: Proc. Lunar Plan. Sci. Conf. XXXIII, Lunar and Planetary Institute, Houston TX, pp. 1417–1418, 2002b.

De Angelis, G., Wilson, J.W., Tripathi, R.K., et al. A radiation analysis of lunar surface habitats. International Astronautics Conference (IAC) 2002, Paper IAC-02-IAA.13.P.09, 2002c.

De Angelis, G., Clowdsley, M.S., Nealy, J.E., et al. Radiation shielding analysis for deep space sessions, in: El-Genk, M. (Ed.), Proceedings of the Space Technology and Application International Forum (STAIF-2003) 'Expanding the Frontiers of Science', AIP Conference Proceedings, New York, pp. 972–983, 2003.

De Angelis, G., Tripathi, R.K., Nealy, J.E., et al. A radiation analysis for lunar surface habitats. COSPAR 35th Scientific Assembly, Paper F2.7-00121, 2004.

Fuji, Z., McDonald, F.B. Radial intensity gradients of galactic cosmic rays (1972–1995) in the heliosphere. J. Geophys. Res. 102 (A11), 24201–24208, 1997.

Hall, D.L., Duldig, M.L., Humble, J.E. Analysis of sidereal and solar anisotropies in cosmic rays. Space Sci. Rev. 17, 401–442, 1996.

Meyer, P., Parker, E.N., Simpson, J.A. Solar cosmic rays of February 1956 and their propagation through interplanetary space. Phys. Rev. 104, 768–781, 1956.

Nymmik, R.A. Models describing solar cosmic ray events. Radiat. Meas. 26, 417–420, 1996.

Parker, E.N. The passage of energetic charged particles through interplanetary space. Planet. Space Sci. 13, 9–49, 1965.

Reames, D.V. Particle acceleration at the sun and in the heliosphere. Space Sci. Rev. 90, 417–491, 1999.

Schaefer, H.J., Radiation and Man in Space. Adv. Space Res. 1, 267–339, 1959.

Shea, M.A., Smart, D.F. History of energetic solar protons for the past three solar cycles including cycle 22 update, in: Swenberg, C.E., Horneck, G., Stassinopoulos, E.G. (Eds.), Biological Effects and Physics of Solar and Galactic Cosmic Radiation. Plenum Press, New York, pp. 37–71, 1993.

Simonsen, L.C., Nealy, J.E., Townsend, L.W., et al. Radiation Exposure for Manned Mars Surface Missions. NASA TP-2979, 1990.

Tripathi, R.K., Wilson, J.W., Cucinotta, F.A., et al. Deep space mission shielding optimization. SAE 2001-01-2326, 2001.

Wilson, J. W., Badavi, F.F., Cucinotta, F.A., et al. HZETRN: Description of a Free-Space Ion and Nucleon Transport and Shielding Computer Program. NASA TP-3495, 1995.

Wilson, J.W., Miller, J., Konradi, A., Cucinotta, F.A. (Eds.), Shielding Strategies for Human Space Exploration. NASA CP-3360, 1997.

Wilson, J.W., Cucinotta, F.A., Shinn, J.L., et al. Shielding from solar particle event exposures in deep space. Radiat. Meas. 30, 361–382, 1999a.

Wilson, J.W., Kim, M.H.Y., Cucinotta, F.A., et al. Variations and Application to the Space Radiation Environment. NASA TP-209369, 1999b.

Wilson, J.W., Clowdsley, M.S., Shinn, J.L., Singleterry, R.C., Tripathi, R.K., Cucinotta, F.A., Heinbockel, J.H., Badavi, F.F., Atwell, W. Neutrons in Space: Shield Models and Design Issues. SAE Paper number 00ICES-377, 2000.

Wilson, J.W., Badavi, F.F., Kim, M.-H., et al. Natural and Induced Environment in Low Earth Orbit. NASA/TM-2002-211668, 2002.

Wilson, J.W., Nealy, J.E., De Angelis, G., et al. Deep space environment and shielding, in: El-Genk, M. (Ed.), Proceedings of the Space Technology and Application International Forum (STAIF-2003) 'Expanding the Frontiers of Science', AIP Conference Proceedings, New York, pp. 993–1009, 2003.

Xapsos, M.A., Barth, J.L., Stassinopoulos, E.G., et al. Space Environment Effects: Model for Emission of Solar Protons (ESP) – Cumulative and Worst-Case Event Fluences. NASA/TP-1999-209763, 1999.